

# Voltage control of magnetic anisotropy in Fe films with quantum well states

Uwe Bauer,<sup>1,\*</sup> Marek Przybylski,<sup>2,3</sup> and Geoffrey S. D. Beach<sup>1</sup>

<sup>1</sup>*Department of Materials Science and Engineering, Massachusetts Institute of Technology, Cambridge, Massachusetts 02139, USA*

<sup>2</sup>*Max-Planck-Institut für Mikrostrukturphysik, Weinberg 2, 06120 Halle, Germany*

<sup>3</sup>*Faculty of Physics and Applied Computer Science, and Academic Centre for Materials and Nanotechnology, AGH University of Science and Technology, al. Mickiewicza 30, 30-059 Krakow, Poland*

(Received 20 January 2014; published 2 May 2014)

The influence of a gate voltage on magnetic anisotropy is investigated in a thin Fe film epitaxially grown on a Ag(1,1,10) substrate and covered by MgO. Oscillations in step-induced magnetic anisotropy due to quantum well states (QWS) confined in the Fe film are observed and shown to persist up to room temperature at low Fe thicknesses. By systematically examining the voltage and thickness dependence of the magnetic hysteresis loop characteristics, we identify two distinct effects by which an applied voltage modifies the magnetic anisotropy. The first effect is due to voltage-induced changes to interfacial perpendicular magnetic anisotropy which, due to the vicinal geometry, leads to changes in the effective in-plane uniaxial magnetic anisotropy. A second effect is observed at lower film thicknesses and shows nonmonotonic voltage-induced effects on magnetic anisotropy. This nonmonotonic behavior coincides with the onset of significant QWS-induced effects on magnetic anisotropy and suggests a link between QWS- and voltage-induced anisotropy changes.

DOI: [10.1103/PhysRevB.89.174402](https://doi.org/10.1103/PhysRevB.89.174402)

PACS number(s): 75.30.Gw, 85.75.-d, 75.70.-i, 73.21.Fg

## I. INTRODUCTION

In thin ferromagnetic films, broken symmetry and spin-orbit coupling at surfaces and interfaces can lead to an interfacial contribution to the magnetic anisotropy energy (MAE) that dominates if the film is sufficiently thin. Interface MAE can be modified by an applied voltage through spin-dependent charge accumulation and band shifting [1–9]. This provides a means to achieve magnetoelectric coupling in thin-film ferromagnetic transition metals, despite the fact that electric fields are screened from the bulk of the material. Apart from one exception [10], studies of magnetoelectric coupling in metals have focused on ferromagnetic-metal/oxide bilayers in which interfacial hybridization at the metal/oxide interface generates perpendicular magnetic anisotropy (PMA) [1–5]. Voltage-induced anisotropy changes have been demonstrated experimentally in such systems [1–5], but significant effects are observed only in films just a few monolayers (MLs) thick near the spin-reorientation transition (SRT), such that small changes in interfacial PMA have a pronounced impact on the net anisotropy.

There exist, however, other electronic effects that are potentially amenable to electrical gating and that could allow voltage control of magnetic anisotropy at higher film thickness. For example, electron confinement along the film normal can lead to quantum well states (QWS) that strongly influence MAE even at film thicknesses of tens of MLs [11–17]. Because magnetic anisotropy is extremely sensitive to the relative occupation of the spin-dependent  $3d$ -bands at the Fermi level ( $E_F$ ), QWS near  $E_F$  can modulate the MAE by modifying the density of available states [17]. Since the QWS energy levels cross  $E_F$  periodically as a function of film thickness [13,17], oscillatory magnetic anisotropy can result if these states couple to and modulate the occupation of the  $3d$  states responsible for generating the MAE. Recently, strong oscillations of

in-plane step-induced anisotropy in Fe films grown on vicinal substrates have been observed and attributed to minority spin  $d$ -band QWS confined within the Fe film [13,14,18]. These oscillations occurred with a period of  $\sim 6$  ML [13–15] and had a significant amplitude even at Fe thicknesses  $d_{\text{Fe}} > 30$  ML [13,15]. The remarkable sensitivity of MAE to small changes of the band structure at  $E_F$ , and the important role of the surface electronic structure in establishing the boundary conditions that confine the QWS, suggest that these systems could provide a new means to control magnetic properties by gating the QWS electrically [19].

Past observations of QWS-induced anisotropy oscillations have been restricted to relatively low temperatures. In this work, we show that in a ferromagnetic metal the influence of QWS on magnetic anisotropy can persist up to room temperature (RT) by using epitaxial Ag(1,1,10)/Fe/MgO films. We systematically examine the effects of a gate voltage ( $V_g$ ) on both interfacial PMA and in-plane anisotropy. We find that voltage-driven changes to in-plane anisotropy can be observed up to  $d_{\text{Fe}} = 25$  ML, and we show that these changes arise from two distinct mechanisms. The first is due to modulation of interfacial PMA which, due to the geometry of the vicinal substrate, results in an in-plane anisotropy that can be tuned by  $V_g$ . However, a second effect with the opposite magnetoelectric polarity dominates at lower  $d_{\text{Fe}}$  and is most pronounced where the influence of QWS on magnetic anisotropy is the strongest. We suggest that this effect may result from voltage-induced modification of the QWS, with a consequent variation of the in-plane magnetic anisotropy. These results demonstrate that magnetoelectric coupling in metals can be used to control in-plane magnetic anisotropy and point to a novel approach to extend magnetoelectric effects beyond the ultrathin film regime through coupling to QWS.

## II. EXPERIMENT

Fe films were grown on a Ag(1,1,10) single-crystal substrate and covered by MgO in a multichamber ultrahigh vacuum (UHV) system with a pressure below  $2 \times 10^{-10}$  mbar

\*ubauer@mit.edu

during Fe and  $9 \times 10^{-10}$  mbar during MgO deposition. Ag(1,1,10) was prepared by cycles of 1 keV Ar ion sputtering and subsequent annealing at  $\sim 870$  K. This resulted in sharp double-split spots in low energy electron diffraction and regular mono-atomic steps with a terrace width of  $\sim 2$  nm, imaged using scanning tunneling microscopy. Ag(1,1,10) exhibits a vicinal angle of  $\alpha = 8^\circ$  with respect to the Ag(001) surface and step edges parallel to the Ag[110] direction [Fig. 1(a)]. Fe grows epitaxially on Ag(1,1,10), and, due to a rotation of the Fe surface net by  $45^\circ$ , the substrate step edges are parallel to the Fe [100] direction.

Fe was deposited by molecular beam epitaxy using a mixed-temperature growth process [20] to avoid Ag segregation at the surface of the Fe film. First, 5 ML of Fe were grown at 140 K as a Ag diffusion barrier, then 24 ML of Fe were deposited at RT in wedge geometry with a slope of  $\sim 4$  ML/mm. A 34-ML-thick shoulder was added to determine the wedge position [21]. After deposition, the film was annealed for 30 minutes at 475 K to improve the surface morphology [22]. Subsequently, a 10-nm-thick MgO capping layer was grown at RT by electron beam evaporation from a stoichiometric MgO rod.

After breaking vacuum, a  $\text{ZrO}_2$  high- $\kappa$  dielectric and transparent indium tin oxide (ITO) electrodes were prepared by dc magnetron sputtering at RT under  $4 \times 10^{-3}$  mbar Ar with a background pressure of  $1 \times 10^{-7}$  mbar [4]. First, 60 nm  $\text{ZrO}_2$  were reactively sputtered from a Zr target at an oxygen partial pressure of  $1.5 \times 10^{-4}$  mbar. Then, an array of 70- $\mu\text{m}$ -diameter, 30-nm-thick ITO electrodes was deposited through a shadow mask from a stoichiometric ITO target.

The temperature-dependent magnetic properties were probed in a liquid-He cryostat-equipped UHV chamber via the longitudinal magneto-optical Kerr effect (MOKE), using a diode laser with 670-nm wavelength and beam diameter of  $\sim 0.2$  mm. The  $V_g$  dependence of magnetic properties was probed *ex situ* at RT via longitudinal MOKE using a diode laser with 532-nm wavelength focused to a  $\sim 5$ - $\mu\text{m}$ -diameter probe spot and positioned with a high-resolution scanning stage. The ITO electrodes were contacted with tungsten cat whisker probes with 1- $\mu\text{m}$ -tip diameter to minimize mechanical contact forces on the sample. The electromagnet could be rotated independently of the sample, which allowed for application of an in-plane magnetic field ( $H$ ) parallel and perpendicular to the step edges of Ag(1,1,10).

### III. RESULTS

#### A. Step-induced anisotropy and thickness-dependent anisotropy oscillations

For a body-centered-cubic (bcc) Fe film on Ag(1,1,10), the orientation of the easy axis is dictated by the balance between shape, perpendicular, fourfold, and step-induced magnetic anisotropy. The anisotropy energy density can then be expressed as [23,24]

$$E = 2\pi M^2 u_z^2 + K_u u_z^2 + K_{4\text{-fold}}(u_x^2 u_y^2 + u_y^2 u_z^2 + u_z^2 u_x^2) + K_{\text{step}} u_y u_z. \quad (1)$$

Here,  $u$  is the unit vector of the magnetization  $M$ ;  $x$ ,  $y'$  and  $z'$  are the [100], [010], and [001] axes, respectively; and  $z$  is the

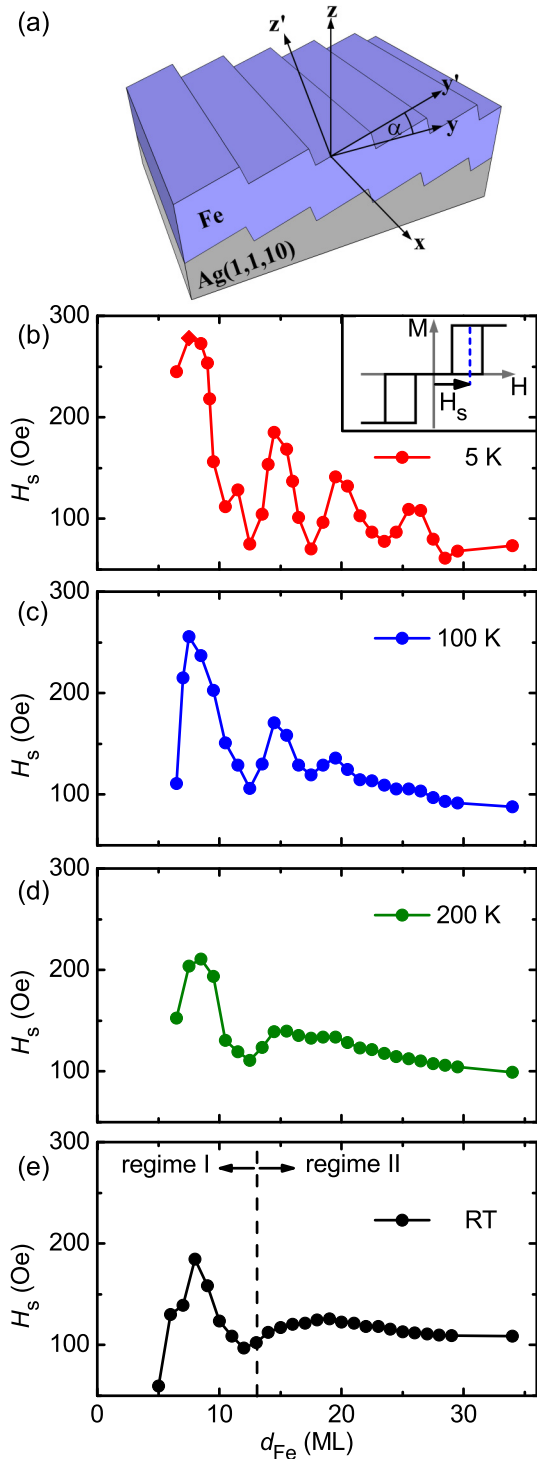


FIG. 1. (Color online) (a) Schematic of Fe film on Ag(1,1,10) substrate. Ag(1,1,10) is miscut by a vicinal angle  $\alpha = 8^\circ$  with respect to the Ag(001) surface. The  $x$ ,  $y'$ , and  $z'$  axes denote the [100], [010], and [001] axes of Fe, respectively. The  $x$  and  $y$  axes define the film plane with the  $x$  axis parallel to the step edges of the Ag(1,1,10) substrate, and  $z$  corresponds to the film normal, which is off the  $z'$  axis by  $\alpha$ . (b)–(e) Fe thickness ( $d_{\text{Fe}}$ ) dependence of shift field  $H_s$  measured at a temperature  $T = 5$  K (b), 100 K (c), 200 K (d), and RT (e). Inset in (b) shows schematic of split hysteresis loop which is characterized by a shift field  $H_s$ . Dashed black line in (e) separates RT thickness dependence of  $H_s$  into two regimes: regime I and regime II.

film normal direction, which is off the [001] axis by  $\alpha = 8^\circ$  [Fig. 1(a)].

For thin Fe films, PMA dominates and pulls the magnetization out of the film plane towards the [001] direction, whereas for thicker Fe films, shape anisotropy dominates and pulls the magnetization towards the film plane. Because the terrace plane and film plane are inclined from one another by  $\alpha$ , this SRT is not an abrupt transition but rather a continuous rotation of the magnetization in the  $yz$  plane toward the film plane (i.e., the  $xy$  plane) [24].

Above the SRT thickness, superposition of fourfold and step-induced anisotropy results in a net uniaxial in-plane anisotropy with the easy axis oriented parallel to the step edges [13,15,24–26]. Therefore, square/split hysteresis loops are measured in longitudinal MOKE if  $H$  is applied parallel/perpendicular to the step edges, respectively. The split loops are characterized by a shift field  $H_s$  [Fig. 1(b), inset], which is typically taken as a measure of the uniaxial in-plane anisotropy [13,24,27].

Figures 1(b)–1(e) show the thickness dependence of  $H_s$  measured at temperatures  $T = 5$  K, 100 K, 200 K, and 300 K. At  $T = 5$  K,  $H_s$  oscillates strongly with a period of  $\sim 6$  ML, and four maxima and minima are clearly distinguished [13–15]. As  $T$  is increased, the anisotropy oscillations are increasingly obscured at higher  $d_{\text{Fe}}$ , likely due to the temperature dependence of the Fermi occupation factor [16,28], but the positions of the maxima and minima are independent of  $T$ .

Previously, thickness-dependent oscillations in  $H_s$  have only been observed at  $T < 200$  K [13,15], while at RT  $H_s$  varied smoothly with  $d_{\text{Fe}}$ , following  $H_s = H_s^{\text{volume}} + H_s^{\text{surf}}/d_{\text{Fe}}$ , where  $H_s^{\text{surf}}$  and  $H_s^{\text{volume}}$  account for surface and volume contributions, respectively [13,15]. Here,  $H_s$  exhibits a strongly nonmonotonic  $d_{\text{Fe}}$  dependence in the low-thickness regime, corresponding to the locations of the first QWS-induced anisotropy maximum and minimum [Fig. 1(e)]. We attribute these QWS-induced anisotropy oscillations at RT to improved surface and interface roughness [16] due to the mixed-temperature growth process and a lower SRT thickness in Fe/MgO. Measurements of split loops at low  $d_{\text{Fe}}$  have previously been hindered by the proximity of the SRT which, for uncovered Fe, occurs at  $\sim 7$  ML at RT [13]. For Fe/MgO, we find a SRT thickness of  $< 5$  ML, consistent with previous results [4] on Ag(001). Due to the lower SRT thickness, split loops could be measured down to 5 ML, revealing the influence of QWS on anisotropy persisting to RT.

Based on these  $T$ -dependent MOKE measurements, the Fe wedge can be separated into two thickness regimes at RT [Fig. 1(e)]. In regime I ( $d_{\text{Fe}} < 13$  ML), magnetic anisotropy is strongly influenced by QWS in the Fe film, whereas in regime II ( $d_{\text{Fe}} > 13$  ML), QWS-induced effects are negligible. Considering the modulation of the electronic band structure at  $E_F$  associated with the presence of QWS, we show in the following that the influence of  $V_g$  on  $H_s$  is distinctly different in regimes I and II.

### B. Voltage-induced magnetic anisotropy changes

The influence of  $V_g$  on magnetic properties was examined at RT using a custom high-resolution scanning MOKE polarimeter with integrated electrical microprobes [4]. Due to charge

trapping effects in the MgO/ZrO<sub>2</sub>/ITO gate structure, negative  $V_g$  has little effect on the magnetic properties [4]. Therefore, we focus on the effects of positive  $V_g$ , which significantly modifies the in-plane hysteresis loop characteristics.

Figure 2 shows loops measured at the center of an ITO electrode for  $V_g = 0$  V and  $V_g = +6$  V. With  $H$  applied parallel to the step edges [Fig. 2(a)], square loops are obtained as expected [13,24,26], and neither the coercivity  $H_c$  nor the saturation Kerr signal  $\phi_s$  are affected by  $V_g$ . The insensitivity of  $H_c$  to  $V_g$  for hysteresis loops along this axis is consistent with nucleation-dominated reversal due to random nucleation sites distributed throughout the film [29]. The lack of voltage-induced changes to  $\phi_s$  indicates that  $M_s$  is unchanged by  $V_g$ , and that  $V_g$  application across the oxide does not introduce optical artifacts that could affect the Kerr rotation or ellipticity.

Hysteresis loops measured perpendicular to the steps are by contrast strongly influenced by  $V_g$ . At  $d_{\text{Fe}} = 10$  ML [Fig. 2(b)],  $H_s$  decreases from  $\sim 90$  Oe to  $\sim 60$  Oe, implying significant voltage effects on in-plane uniaxial anisotropy. Moreover,  $\phi_s$  is reduced to  $\sim 40\%$  of its initial value. Since parallel to the steps  $\phi_s$  is unchanged by  $V_g$  [Fig. 2(a)], this is not due to changes in  $M_s$ , but rather a reduction in interfacial PMA, which affects  $\phi_s$  due to the vicinal geometry [14,30,31]. Since the PMA is not orthogonal to the shape anisotropy, it can tilt the magnetization out of the film plane and stabilize an out-of-plane magnetization component beyond the SRT thickness. And since the polar MOKE effect is about one order

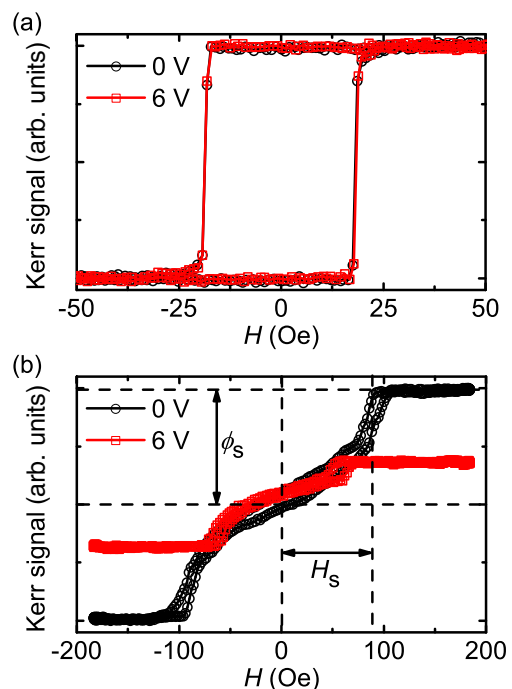


FIG. 2. (Color online) (a) Representative hysteresis loops measured by MOKE at  $d_{\text{Fe}} = 11$  ML with the magnetic field  $H$  applied parallel to the step edges at a gate voltage of  $V_g = 0$  V and  $V_g = 6$  V. (b) Representative split hysteresis loops at  $d_{\text{Fe}} = 10$  ML with  $H$  applied perpendicular to the step edges at  $V_g = 0$  V and  $V_g = 6$  V. The split loops are characterized by a shift field  $H_s$  and a Kerr signal in saturation  $\phi_s$ , which are indicated here for the split loop measured at  $V_g = 0$  V.

of magnitude larger than the longitudinal MOKE effect [32], even a small out-of-plane component can significantly modify  $\phi_s$ .  $\phi_s$  increases/decreases depending on whether the polar MOKE signal adds/subtracts from the longitudinal, which depends on the measurement geometry and is further described below [14,30,31].

By contrast, in the  $xz$  plane, PMA and shape anisotropy remain orthogonal even for the vicinal substrate, and the magnetization is not tilted out of the film plane [24]. Therefore, no out-of-plane component is observed above the SRT thickness, and the square loops measured parallel to the step edges are unaffected by PMA [13,26].

Figure 3 shows the  $V_g$  dependence of  $H_c$ ,  $H_s$ , and  $\phi_s$  at  $d_{\text{Fe}} = 15$  ML, which was measured continuously as  $V_g$  was ramped from 0 V to 6 V in 0.2 V steps every  $\sim 60$  s [Fig. 3(d)]. Up to  $V_g = 4$  V,  $H_s$  increases by 2 Oe but then decreases sharply by 14 Oe until it saturates at  $V_g = 6$  V [Fig. 3(a)]. For  $H$  parallel to the step edges,  $H_c$  remains unchanged [Fig. 3(b)]. Similar behavior was observed at all  $d_{\text{Fe}}$ , with the maximum of  $H_s$  typically occurring between  $V_g = 3$  V to 4 V. We refer to this maximum of  $H_s$  as  $H_{s,+}$  and the difference between  $H_s$  at 0 V and  $H_{s,+}$  as  $\Delta H_{s,+}$ . Similarly, we refer to the minimum in the  $V_g$  response of  $H_s$ , usually occurring at  $V_g = 6$  V, as  $H_{s,-}$  and the difference between  $H_s$  at 0 V and  $H_{s,-}$  as  $\Delta H_{s,-}$  [Fig. 3(a)]. The change in sign of  $\Delta H_s$ , which coincides with the onset of nonlinear charge-trapping effects in the oxide [4], could indicate the presence of two competing contributions to  $H_s$  with opposite sign and different  $V_g$  dependence.

Figure 3(c) shows the corresponding behavior for  $\phi_s$ , which initially decreases slowly but then drops more rapidly above  $\sim 4$  V and saturates at 6 V,  $\sim 40\%$  below its value at 0 V. However, after rotating the sample by  $180^\circ$  in the film plane, the opposite behavior is observed. Now,  $\phi_s$  increases by  $\sim 40\%$  when  $V_g$  is ramped up to 6 V. Therefore, the modification of  $\phi_s$ , i.e.,  $\Delta\phi_s$ , is indeed due to modification of the out-of-plane magnetization component stabilized by the PMA. The out-of-plane component changes from being additive to being subtractive to  $\phi_s$  under rotation of  $180^\circ$ , explaining the different sign of  $\Delta\phi_s$  [14,30,31]. We will refer to the maximum change in  $\phi_s$  at  $V_g = 6$  V as  $\Delta\phi_{s,6V}$ .

To show that the voltage effects on  $H_s$  and  $\phi_s$  originate from changes at the Fe/MgO interface, 1 ML of Au was sandwiched between the Fe and MgO layers on half of the substrate. Fig. 3(a) shows that this Au ML screens the voltage-induced effects on  $H_s$  almost completely, confirming their origin. This is consistent with the assumption that magnetoelectric effects in metallic ferromagnets are limited to the topmost ML due to the low screening length in metals [6,7]. Since an Ag segregation layer at the Fe surface could result in similar screening effects, avoiding Ag segregation through the mixed-temperature growth process is crucial.

Finally, we performed similar measurements to those shown in Fig. 3 along the Fe wedge by measuring on ITO electrodes spaced  $250 \mu\text{m}$  or  $d_{\text{Fe}} = 1$  ML apart. Figure 4 shows the  $d_{\text{Fe}}$  dependence of  $H_s$ ,  $H_{s,+}$ , and  $H_{s,-}$  (4a),  $\Delta H_{s,+}$  and  $\Delta H_{s,-}$  (4b), and  $\Delta\phi_{s,6V}$  (4c). We note that  $H_s$  in Fig. 4(a) is  $\sim 25\%$  lower as compared to the data in Fig. 1(e), which we attribute to differences in  $H$  calibration,  $H$  sweep rate, and laser spot size of the two MOKE systems. We find that even at the thick end of the Fe wedge,  $H_s$  can be modified by  $V_g$  [Fig. 4(b)].

Starting from this end, where  $\Delta H_{s,-} = -1$  Oe at  $d_{\text{Fe}} = 29$  ML,  $\Delta H_{s,-}$  decreases smoothly and steadily to 15 Oe at 13 ML. Below 13 ML,  $\Delta H_{s,-}$  decreases rapidly, and its absolute value reaches a maximum of 30 Oe at 10 ML. Surprisingly,  $\Delta H_{s,-}$  then increases below 10 ML, and its absolute value reaches a local minimum of 15 Oe at 8 ML. Compared to  $\Delta H_{s,-}$ , voltage effects on  $\Delta H_{s,+}$  are smaller and occur only for  $d_{\text{Fe}} < 17$  ML. Moreover,  $\Delta H_{s,+}$  increases continuously with decreasing  $d_{\text{Fe}}$  and reaches 8 Oe at 8 ML.

Even on the shoulder of the Fe wedge ( $d_{\text{Fe}} = 34$  ML),  $V_g = 6$  V results in a reduction of  $\phi_s$  of  $\sim 20\%$  [Fig. 4(c)]. With decreasing thickness, the absolute value of  $\Delta\phi_{s,6V}$  increases slowly and reaches  $\sim 50\%$  at 13 ML. Below 13 ML however, the absolute value of  $\Delta\phi_s$  increases and reaches a maximum of  $\sim 80\%$  at 8 ML before decreasing again for

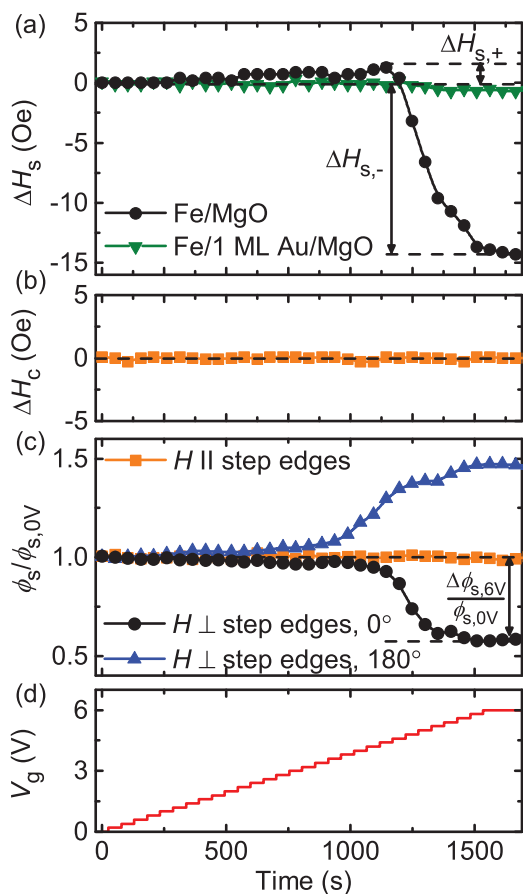


FIG. 3. (Color online) (a) Modification of the shift field  $H_s$  (i.e.,  $\Delta H_s$ ) for Ag(1,1,10)/Fe/MgO/ZrO<sub>2</sub> and Ag(1,1,10)/Fe/1ML Au/MgO/ZrO<sub>2</sub> as the gate voltage  $V_g$  is ramped up from 0 V to 6 V over time.  $\Delta H_{s,+}$  denotes the difference between  $H_s$  at 0 V and the maximum of  $H_s$  in the voltage dependence. Correspondingly,  $\Delta H_{s,-}$  denotes the difference between  $H_s$  at 0 V and the minimum of  $H_s$  in the voltage dependence. (b) Modification of the coercive field  $H_c$  (i.e.,  $\Delta H_c$ ) of square loops measured with the magnetic field  $H$  parallel to the step edges as  $V_g$  is ramped up over time. (c) Relative change of Kerr signal in saturation  $\phi_s$  with  $V_g$  for split loops measured with  $H$  perpendicular to step edges, before and after a  $180^\circ$  rotation of the sample, and change of  $\phi_s$  for square loops measured with  $H$  parallel to step edges.  $\Delta\phi_{s,6V}$  denotes the modification of  $\phi_s$  at  $V_g = 6$  V with respect to its value at 0 V. (d) Time dependence of the applied  $V_g$ .

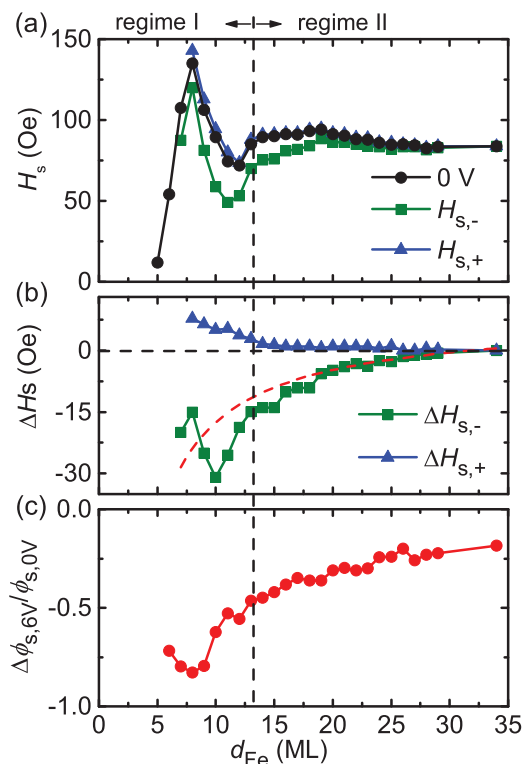


FIG. 4. (Color online) (a) Fe thickness ( $d_{\text{Fe}}$ ) dependence of the shift field  $H_s$  at a gate voltage of 0 V as well as the  $d_{\text{Fe}}$  dependence of the maximum ( $H_{s,+}$ ) and minimum ( $H_{s,-}$ ) of the voltage dependence of  $H_s$ . (b)  $d_{\text{Fe}}$  dependence of the modification of  $H_s$  at the maximum ( $\Delta H_{s,+}$ ) and minimum ( $\Delta H_{s,-}$ ) of the voltage dependence of  $H_s$ . The dashed red curve is an extrapolation of the  $1/d_{\text{Fe}}$  dependence fitted to the data points at  $d_{\text{Fe}} \geq 20$  ML. (c)  $d_{\text{Fe}}$  dependence of the relative modification of the saturation Kerr signal at 6 V, i.e.,  $\Delta\phi_{s,6V}$ . The vertical dashed black line separates the thickness dependence of  $H_s$  into two regimes: regime I and II.

thinner films. Between 13 ML and 34 ML,  $\Delta\phi_s$  is well fit by a  $1/d_{\text{Fe}}$  dependence, as expected for voltage-induced changes to interfacial PMA.

Comparing Figs. 4(b) and 4(c) with 4(a), we find significant differences between the voltage response in regime I ( $d_{\text{Fe}} < 13$  ML) and regime II ( $d_{\text{Fe}} > 13$  ML). In regime II,  $\Delta H_{s,-}$ ,  $\Delta H_{s,+}$ , and  $\Delta\phi_{s,6V}$  have very smooth thickness dependence, and their absolute values decrease, as expected for a surface mediated effect, with increasing thickness. In regime I, however,  $\Delta H_{s,-}$  and  $\Delta\phi_{s,6V}$  show clear maxima and minima. In particular, the local minimum of the absolute value of  $\Delta H_{s,-}$  and the maximum of the absolute value in  $\Delta\phi_{s,6V}$  coincide exactly with the local maximum of  $H_s$  at 8 ML. The difference in voltage response in the two regimes could be an indication that the presence of QWS in regime I modifies the magnetoelectric response of the Fe film.

#### IV. DISCUSSION

We found that  $V_g$  can strongly modify  $H_s$  and  $\phi_s$  of the split hysteresis loops and observed voltage-induced effects even at the highest investigated  $d_{\text{Fe}}$  of 34 ML [Figs. 4(b), 4(c)]. This is surprising considering that in systems with out-of-plane

uniaxial anisotropy, voltage-induced anisotropy changes are usually only observed for films of a few ML [1–5]. In contrast to the simple uniaxial PMA case, the magnetization orientation in Ag(1,1,10)/Fe/MgO is determined by four MAE terms (Eq. 1) whose principal axes are not all collinear nor orthogonal. Due to this complex combination of anisotropies, it is not immediately apparent which contributions are modified by  $V_g$ . In the following, we consider several mechanisms by which  $V_g$  could give rise to the experimental observations.

Under  $V_g$  application,  $\Delta\phi_s$  is positive, null, or negative depending on the sample orientation [Fig. 3(c)], showing that  $M_s$  and, hence shape anisotropy, changes negligibly with  $V_g$ , but interfacial PMA changes significantly. We previously reported a large reduction in PMA under positive  $V_g$  in Ag(001)/Fe/MgO [4], so observing a similar effect in Ag(1,1,10)/Fe/MgO is not surprising. Here, the influence of  $V_g$  on PMA is evident for the nominally in-plane magnetized film due to the large polar MOKE contribution to  $\phi_s$  that arises from a small out-of-plane magnetization component. Since  $\phi_s$  changes monotonically as  $V_g$  is ramped from 0 V to 6 V [Fig. 3(c)], PMA also decreases monotonically with  $V_g$ , consistent with previous results [4] on Ag(001).

We note that the nonlinear dependence of  $\phi_s$  on  $V_g$  [Fig. 3(c)], with rapid change occurring above  $\sim 3$  V and saturation above  $\sim 5$  V, is likely due to nonlinear charge-trapping effects in the oxide stack rather than an intrinsic nonlinear magnetoelectric response. These effects were characterized in Ref. [4], where it was shown that above a threshold voltage, charge trapping in the oxide leads to a dramatic increase in the effective electric field, which saturates at  $V_g \sim 6$  V.

Since PMA is aligned along the  $z'$  axis [Fig. 1(a)], it has a component in the film plane, which contributes to the in-plane anisotropy. Voltage-induced changes to PMA are therefore expected to modify  $H_s$ . To better understand this effect, we consider only PMA and shape anisotropy in Eq. 1 and add a  $V_g$  dependence to PMA:

$$E = 2\pi M^2 u_z^2 + (1 + \alpha V_g) K_u u_z^2. \quad (2)$$

Here  $\alpha$  is a magnetoelectric coefficient that characterizes the voltage response of the PMA. Using  $M = 1710$  G,  $K_u = K_s/d_{\text{Fe}}$ , and  $K_s = 1.6$  erg/cm<sup>2</sup>, we computed the MAE contours shown in Fig. 5. Figure 5(a) shows a cut through the anisotropy energy surface in the  $yz$  plane for  $d_{\text{Fe}} = 8$  ML. The axis along which the anisotropy energy is at a minimum corresponds to the preferred orientation of the magnetization vector in this plane. At 0 V, this minimum energy axis does not coincide with the  $y$  axis but is tilted toward the  $z$  axis, which gives rise to an out-of-plane magnetization component. With increasing  $V_g$ , PMA and the angle between the minimum energy axis and the  $y$  axis decreases, and hence the out-of-plane magnetization component decreases as well [Fig. 5(a)]. Since the split loops are measured with  $H$  applied along the  $y$  axis, this effect gives rise to the observed voltage-induced modification of  $\phi_s$ , due to the combination of longitudinal and polar MOKE signals measured in this geometry. In contrast, in the  $xz$  plane [Fig. 5(b)], the minimum energy axis always coincides with the  $x$  axis, independent of  $V_g$  and PMA. Therefore, no out-of-plane magnetization component and no voltage modification of  $\phi_s$

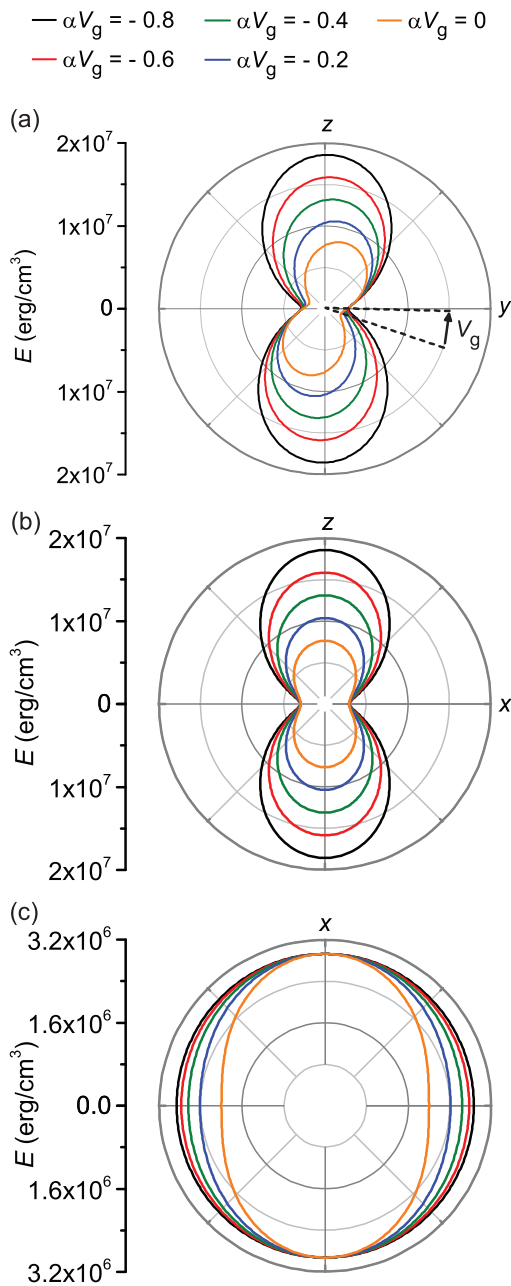


FIG. 5. (Color online) Cuts through the anisotropy energy density ( $E$ ) surface of a 8-ML-thick Fe film on Ag(1,1,10), considering shape and perpendicular magnetic anisotropy. An isotropic contribution of  $M_s^2$  was added for clarity, (a) cut through the  $yz$  plane of  $E$ , (b) cut through the  $xz$  plane of  $E$ , and (c) cut through the minimum energy plane of  $E$  defined by the minimum energy axes in (a) and (b). The dashed black line in (a) shows the voltage dependence of the orientation of the minimum energy axis.

is observed for the square loops measured along the  $x$  axis [Fig. 3(c)].

A cut through the energy surface in the plane defined by the  $x$  axis, and the minimum energy direction in the  $yz$  plane shows that PMA also gives rise to a uniaxial anisotropy in this plane [Fig. 5(c)]. The easy axis of this effective in-plane anisotropy is perpendicular to the  $x$  axis and with decreasing PMA, i.e., increasing  $V_g$ , the uniaxial anisotropy becomes

weaker and eventually disappears. The origin of this uniaxial anisotropy is purely geometrical and a direct consequence of the stepped substrate. Superposition of this contribution from PMA, fourfold anisotropy and step-induced anisotropy then determines the difference between the anisotropy energy parallel and perpendicular to the step edges, which gives rise to  $H_s$ . Since the contribution from PMA favors an alignment of the magnetization perpendicular to the step edges, an increase in  $V_g$  would increase the MAE along this direction and enhance  $H_s$ . And indeed, this increase in  $H_s$  is observed up to 4 V in Fig. 3(a) and shown as  $\Delta H_{s,+}$  in Fig. 4(b).

Voltage-induced reduction of PMA explains the modification of  $\phi_s$  and the increase in  $H_s$ , which occurs up to 4 V. However, the monotonic decrease of PMA cannot account for the nonmonotonic change in  $H_s$ , namely the large decrease observed above 4 V [Fig. 3(a)]. Therefore  $V_g$  must also modify the other anisotropy contributions. Considering the high sensitivity of the step-induced anisotropy to step-decoration and overlayer material [13,33–35], it is the most likely candidate to show strong voltage effects. Due to the presence of steps at the Fe/MgO interface, a voltage could directly modify the step-induced anisotropy by modulating the charge density at the steps. However, the step-induced anisotropy also depends strongly on the QWS in the Fe film [Fig. 1(e)], and voltage-induced modification of the nature of the QWS could indirectly modify the anisotropy. Likely, both effects occur and simultaneously modify electronic structure and step-induced anisotropy. It is difficult to separate their relative contributions, but the presence of the pronounced maximum and minimum in  $\Delta H_{s,-}$  at  $d_{\text{Fe}} < 13$  ML [Fig. 4(b)] suggests that QWS play an important role. Above 20 ML,  $\Delta H_{s,-}$  is well fit by a  $1/d_{\text{Fe}}$  dependence. Assuming that no QWS effects occur above 20 ML, we can estimate an upper limit of the direct voltage-induced effect by extrapolating the  $1/d_{\text{Fe}}$  dependence to lower thickness [Fig. 4(b)]. This very rough estimate shows that the direct voltage-induced effect is insufficient to account for the large modifications of  $H_s$  at low  $d_{\text{Fe}}$  and confirms that QWS-induced effects play a significant role.

Voltage application, amplified by nonlinear charge trapping effects in the oxide above 4 V [4] could modify the boundary conditions at the Fe/MgO interface and directly influence the QWS in the Fe film [36]. Since oscillations of the density of states close to  $E_F$  associated with the  $d$ -band QWS lead to large-amplitude modulations of the step-induced anisotropy, even small changes in these states could have a significant impact on  $H_s$ . In a simple model, the effect of  $V_g$  on QWS can be described as a change in effective thickness of the Fe film. Within this model, the voltage-induced modification of  $H_s$  should change in polarity at Fe thicknesses corresponding to a maximum or minimum of  $H_s$ , which is not exactly what we observe experimentally (Fig. 4). Therefore, additional experiments and theoretical studies are necessary to clearly identify and better understand the interplay between voltage-induced effects and QWS in ferromagnetic metal films. Nevertheless, our study indicates that such a connection likely exists and could be exploited to engineer and enhance magnetoelectric coupling in ferromagnetic metal films at RT.

## V. SUMMARY

In summary, we have investigated voltage-induced effects on magnetic anisotropy of Fe films grown on a Ag(1,1,10) substrate in a thickness range of 5 ML to 34 ML. We show that anisotropy oscillations due to QWS in the Fe film can persist up to RT and strongly influence the in-plane anisotropy. Moreover, we demonstrate that PMA can be controlled by a gate voltage up to 34 ML of Fe and find that this effect can be exploited to control in-plane anisotropy, due to the vicinal substrate. In addition, we observe a second contribution to the voltage-induced anisotropy modification that results in large nonmonotonic changes of the in-plane anisotropy. The nonmonotonic behavior coincides with the onset of significant QWS-induced effects on magnetic anisotropy and suggests a

link between the QWS-modulated electronic structure of the Fe film and its voltage response. These results open up a new degree of freedom in voltage control of magnetism, employing electron confinement and the associated modulation of electronic band structure to better understand, engineer, and enhance magnetoelectric effects in ferromagnetic transition metals.

## ACKNOWLEDGMENTS

This work was supported by the National Science Foundation under Grant No. NSF-ECCS -1128439. Technical support from David Bono, Mike Tarkanian, and W. Greie is gratefully acknowledged. We are also grateful to J. Kirschner for useful discussions and M. Cinal for his valuable comments.

- 
- [1] M. Weisheit, S. Fahler, A. Marty, Y. Souche, C. Poinsignon, and D. Givord, *Science* **315**, 349 (2007).
  - [2] T. Maruyama, Y. Shiota, T. Nozaki, K. Ohta, N. Toda, M. Mizuguchi, A. A. Tulapurkar, T. Shinjo, M. Shiraishi, S. Mizukami, Y. Ando, and Y. Suzuki, *Nat. Nanotechnol.* **4**, 158 (2009).
  - [3] M. Endo, S. Kanai, S. Ikeda, F. Matsukura, and H. Ohno, *Appl. Phys. Lett.* **96**, 212503 (2010).
  - [4] U. Bauer, M. Przybylski, J. Kirschner, and G. S. D. Beach, *Nano Lett.* **12**, 1437 (2012).
  - [5] D. Chiba, S. Fukami, K. Shimamura, N. Ishiwata, K. Kobayashi, and T. Ono, *Nat. Mater.* **10**, 853 (2011).
  - [6] C. G. Duan, J. P. Velev, R. F. Sabirianov, Z. Q. Zhu, J. H. Chu, S. S. Jaswal, and E. Y. Tsymlal, *Phys. Rev. Lett.* **101**, 137201 (2008).
  - [7] M. K. Niranjan, C. G. Duan, S. S. Jaswal, and E. Y. Tsymlal, *Appl. Phys. Lett.* **96**, 222504 (2010).
  - [8] M. Tsujikawa and T. Oda, *Phys. Rev. Lett.* **102**, 247203 (2009).
  - [9] K. Nakamura, R. Shimabukuro, Y. Fujiwara, T. Akiyama, T. Ito, and A. J. Freeman, *Phys. Rev. Lett.* **102**, 187201 (2009).
  - [10] K. Ohta, T. Maruyama, T. Nozaki, M. Shiraishi, T. Shinjo, Y. Suzuki, S. S. Ha, C. Y. You, and W. Van Roy, *Appl. Phys. Lett.* **94**, 032501 (2009).
  - [11] C. Wursch, C. Stamm, S. Egger, D. Pescia, W. Baltensperger, and J. S. Helman, *Nature* **389**, 937 (1997).
  - [12] W. Weber, A. Bischof, R. Allenspach, C. Wursch, C. H. Back, and D. Pescia, *Phys. Rev. Lett.* **76**, 3424 (1996).
  - [13] J. Li, M. Przybylski, F. Yildiz, X. D. Ma, and Y. Z. Wu, *Phys. Rev. Lett.* **102**, 207206 (2009).
  - [14] J. Li, M. Przybylski, Y. He, and Y. Z. Wu, *Phys. Rev. B* **82**, 214406 (2010).
  - [15] U. Bauer and M. Przybylski, *Phys. Rev. B* **81**, 134428 (2010).
  - [16] U. Bauer, M. Dabrowski, M. Przybylski, and J. Kirschner, *Phys. Rev. B* **84**, 144433 (2011).
  - [17] M. Cinal, *J. Phys.: Condens. Matter* **15**, 29 (2003).
  - [18] J. Li, G. Chen, Y. Z. Wu, E. Rotenberg, and M. Przybylski, *IEEE Trans. Magn.* **47**, 1603 (2011).
  - [19] T. R. Dasa, P. Ruiz-Diaz, O. O. Brovko, and V. S. Stepanyuk, *Phys. Rev. B* **88**, 104409 (2013).
  - [20] D. E. Burgler, C. M. Schmidt, D. M. Schaller, F. Meisinger, R. Hofer, and H. J. Guntherodt, *Phys. Rev. B* **56**, 4149 (1997).
  - [21] U. Bauer, J. Choi, J. Wu, H. Chen, and Z. Q. Qiu, *Phys. Rev. B* **76**, 184415 (2007).
  - [22] Z. Q. Qiu, J. Pearson, and S. D. Bader, *Phys. Rev. Lett.* **70**, 1006 (1993).
  - [23] D. S. Chuang, C. A. Ballentine, and R. C. O'Handley, *Phys. Rev. B* **49**, 15084 (1994).
  - [24] R. K. Kawakami, E. J. Escorcia-Aparicio, and Z. Q. Qiu, *Phys. Rev. Lett.* **77**, 2570 (1996).
  - [25] B. Heinrich, S. T. Purcell, J. R. Dutcher, K. B. Urquhart, J. F. Cochran, and A. S. Arrott, *Phys. Rev. B* **38**, 12879 (1988).
  - [26] Y. Z. Wu, C. Won, and Z. Q. Qiu, *Phys. Rev. B* **65**, 184419 (2002).
  - [27] W. Weber, C. H. Back, A. Bischof, C. Wursch, and R. Allenspach, *Phys. Rev. Lett.* **76**, 1940 (1996).
  - [28] M. Przybylski, M. Dabrowski, U. Bauer, M. Cinal, and J. Kirschner, *J. Appl. Phys.* **111**, 07C102 (2012).
  - [29] U. Bauer, S. Emori, and G. S. D. Beach, *Appl. Phys. Lett.* **100**, 192408 (2012).
  - [30] Y. Z. Wu, C. Won, H. W. Zhao, and Z. Q. Qiu, *Phys. Rev. B* **67**, 094409 (2003).
  - [31] U. Bauer, M. Dabrowski, M. Przybylski, and J. Kirschner, *J. Magn. Magn. Mater.* **323**, 1501 (2011).
  - [32] J. Zak, E. R. Moog, C. Liu, and S. D. Bader, *J. Magn. Magn. Mater.* **89**, 107 (1990).
  - [33] W. Weber, C. H. Back, A. Bischof, D. Pescia, and R. Allenspach, *Nature* **374**, 788 (1995).
  - [34] R. K. Kawakami, M. O. Bowen, H. J. Choi, E. J. Escorcia-Aparicio, and Z. Q. Qiu, *Phys. Rev. B* **58**, R5924 (1998).
  - [35] H. C. Mireles and J. L. Erskine, *J. Appl. Phys.* **93**, 7139 (2003).
  - [36] M. Milun, P. Pervan, and D. P. Woodruff, *Rep. Prog. Phys.* **65**, 99 (2002).